ACS APPLIED MATERIALS & INTERFACES

Research Article

www.acsami.org

All-Optical Technique to Correlate Defect Structure and Carrier Transport in Transferred Graphene Films

Caitlin Rochford,*,† Nardeep Kumar, Jianwei Liu, Hui Zhao, and Judy Wu*

Department of Physics and Astronomy, University of Kansas, Lawrence, Kansas 66045, United States

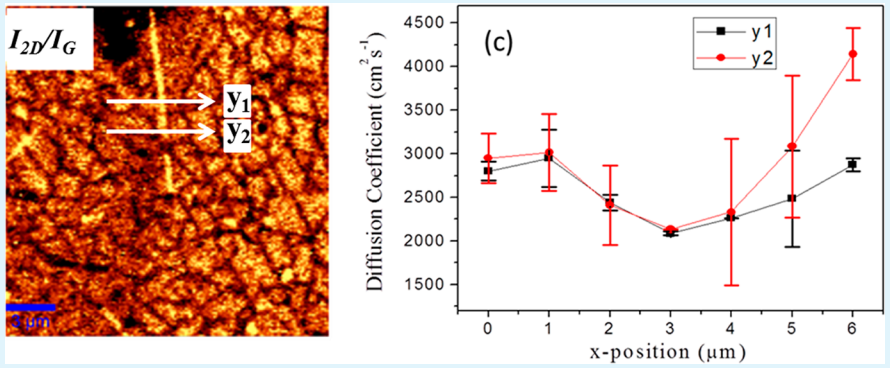

ABSTRACT: Chemical vapor deposition of graphene on copper foil is an attractive method of producing large-area graphene films, but the electronic performance is limited by defects such as creases from the film transfer process, wrinkles due to the thermal expansion coefficient mismatch, and grain boundaries from the growth process. Here we present an all-optical technique to correlate defect structure with electronic properties using spatially resolved Raman spectroscopy and transient absorption microscopy. This technique is especially attractive since it does not require any lithographic steps to probe the electronic properties of the graphene film. As a first demonstration, we focus on the effects of both wrinkles and creases while averaging over many small grains. It was found that wrinkles and creases may decrease the charge carrier diffusion coefficient by over 50% due to increased defect scattering. This technique may easily be extended to large grain graphene films in order to study the effect of different types of grain boundaries.

KEYWORDS: *graphene, transient absorption microscopy, chemical vapor deposition, grain boundaries, defects, Raman spectroscopy*

INTRODUCTION

Much of the excitement surrounding graphene is due to the extraordinary electrical properties established on exfoliated graphene flakes which are single crystalline and have minimal defects. However, if graphene is to be utilized commercially, large area films compatible with standard lithographic techniques are needed. Growth of graphene by chemical vapor deposition (CVD) on copper foil has emerged as an extremely promising method of producing large area single layer graphene films, yet the electronic properties suffer greatly from various defects. The structure of the defects and the nature of their effect on carrier transport must be understood in order to optimize graphene film fabrication and make large area graphene competitive. In this work, we present an all-optical technique to correlate defect structure with carrier diffusion. Because of the complications induced by the fabrication steps necessary to pattern graphene and deposit metal electrodes as well as the influence of electrode material and contact quality on electronic measurements, an optical technique is highly advantageous.

Graphene sheets were grown on a 25 μm thick copper foil (Alfa Aesar, item No.13382) by chemical vapor deposition (CVD) at 1000 °C following previously published procedures.[1,2] In order to transfer the CVD-grown graphene films onto the desired substrate, poly methyl methacrylate (PMMA) was first spin-coated on the surface of the as-grown graphene on copper. The film was then placed into iron chloride solution (0.1g/mL) to remove the copper foil, rinsed in deionized (DI) water three times, and allowed to soak in 2 L fresh DI water overnight to further remove remaining iron and copper residuals. The target substrate (BK7 glass) was then immersed into the DI water and used to lift the graphene film from the liquid. The sample was placed into an oven in air at 80 °C for 1 h for drying. PMMA was then redeposited and allowed to cure slowly overnight. This second PMMA step helps to reduce cracking in the graphene. Finally, the PMMA was removed with hot acetone. PMMA was then spun on again, and identification marks were patterned by electron beam lithography on top of the graphene in order to reproducibly locate specific features. The samples were cleaned by thermal annealing in flowing hydrogen and argon gas at 400 °C for 15 min in order to remove polymer residue from the film transfer and lithography

Received: April 24, 2013
Accepted: July 15, 2013
Published: July 15, 2013

 © 2013 American Chemical Society

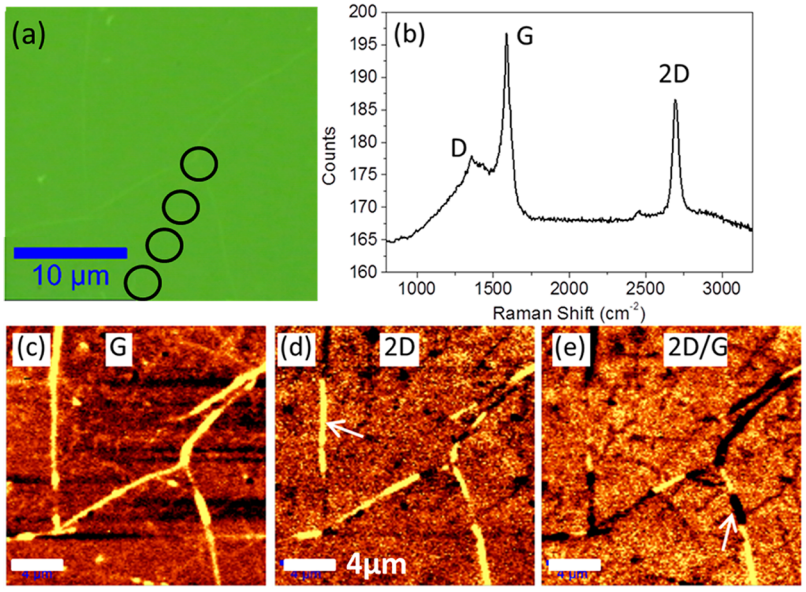

Figure 1. (a) Optical image of graphene transferred to glass. The green tint is from the Raman filter. The black circles correspond to the positions of the diffusion measurements in Figure 2. (b) Average Raman spectra away from the creases. (c and d) Maps of the intensities of the G peak, 2D peak, and 2D/G ratio, respectively.

processes. Potential regions of interest were first identified optically. Confocal Raman mapping was performed in order to characterize the structure of the graphene film (Witec Alpha 300). The Raman system utilized a 488 nm excitation laser with a beam spot of approximately 330 nm, and spectra were taken at a rate of 8 points per micrometer. The laser energy was kept low (~1.5 mW) to avoid sample heating. The charge carrier transport in the Raman-mapped areas was then studied optically by transient absorption microscopy. The results are discussed further below.

RESULTS AND DISCUSSION

Graphene grown by CVD on copper and transferred to an arbitrary substrate using the above method will contain three different types of boundaries which vary in origin and characteristic size. The first and most fundamental are grain boundaries which occur when grains of different crystal orientations coalesce during growth, as described above. These domains vary greatly in size from $<10^2$ nm to $>10^2$ μm depending on the copper substrate and the growth conditions. The second are wrinkles due to the difference in thermal expansion coefficient of graphene and copper.[1] Graphene has a large negative thermal expansion coefficient of -6×10^{-6}/K at 27 °C while copper has a large positive thermal expansion coefficient of 24×10^{-6}/K.[3] This suggests that there will be significant shrinkage of copper relative to graphene with cooling. This induces mechanical stress on graphene resulting in the formation of wrinkles. These wrinkles may span multiple graphene grains and define closed domains which are typically a few to a few tens of micrometers in size. The third and least fundamental type of boundary is creases formed during the graphene film transfer process. These large features are visible by optical microscopy and do not necessary form closed domains. Of these three types of boundaries, only the effect of grain boundaries on electronic transport properties has received significant attention.[4−6] All three types of boundaries, however, may have a deleterious effect and therefore must be characterized and understood.

An optical image of the first region under study is shown in Figure 1a. The primary visible features are the creases. The average Raman spectrum over the areas more than 2 μm away from any creases is shown in Figure 1b. The 2D peak is sharp and symmetric. The values of the full width at half-maximum (fwhm) of the 2D peak form a Gaussian-like distribution around a fwhm of 43 cm^{-1}. The ratio of the intensity of the 2D peak to G peak is low compared to mechanically exfoliated monolayer graphene flakes but is not uncommon among values observed in CVD-grown graphene. This is because the G peak signal is enhanced due to the presence of regions with more than one graphene layer[7] and carbon-based residue which was not fully removed during the annealing step. A high doping level may also be responsible and will be discussed further below. Maps of the G peak intensity (I_G), 2D peak intensity (I_{2D}), and the ratio of the 2D peak to G peak intensities (I_{2D}/I_G) are shown in Figure 1c−e, respectively.

It is clear from Figure 1c−e that the creases are not uniform and contain many distinct features. Analysis of the Raman spectra of the different regions reveals a wide variety of structural characteristics. For example, the region marked with the white arrow in Figure 1e has the lowest ratio of D peak intensity to G peak intensity (I_D/I_G) and consists of several layers of high crystalline quality graphene. The bright yellow regions within the creases of Figure 1e consist of single layer graphene as evidenced by large I_{2D}/I_G ratio. One possible reason that these regions show an enhanced I_{2D}/I_G compared to the surrounding graphene could be because they are slightly suspended during the drying process. Ni et al. found that suspended graphene had a higher 2D peak intensity due to the absence of substrate charged impurities which increase carrier density and electron or hole inelastic scattering rate which in turn reduce I_{2D}.[8] The region marked with the white arrow in Figure 1d displays a large I_{2D} and I_G, such that the ratio is indistinguishable from the surrounding graphene. This is may be due to an interference effect which enhances Raman band intensity due to multiple reflections of the laser or the Raman signal itself.[9] The remaining dark regions within the creases of

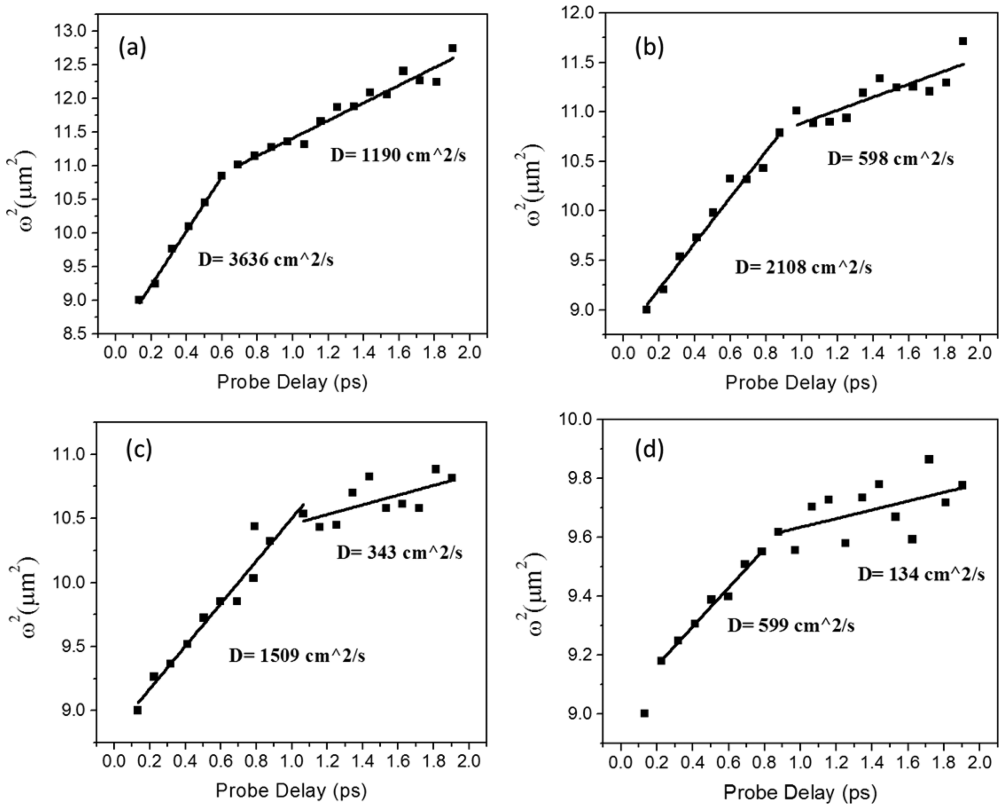

Figure 2. Measurements of diffusion coefficient at the four locations marked in Figure 1a. Carrier profile width squared is plotted against probe delay time so that the slope is equal to the diffusion coefficient. Plots a–d sequentially approach the intersection of the creases so that a is the furthest away and d is directly on top of the intersection.

Figure 1e contain an enhanced G peak, suggesting multiple layers, possibly due to folding.

In addition to the prominent creases, fainter boundaries separating regions of approximately 2–6 μm in size are visible in Figure 1c–e. These are suspected to be the wrinkles due to the difference in thermal expansion of graphene and copper. Corresponding features are visible in Raman maps of graphene on copper (not shown) indicating that they are intrinsic to the growth process and not due to the transfer. The wrinkles are most visible in Figure 1e and are also clear in the map of the 2D peak position (not shown), in which they are shifted to lower wave numbers. The map of the G peak position (not shown), however, is completely featureless. The positions of both the G and 2D peaks in graphene have been shown to be sensitive to doping level,[10,11] with both peaks shifting with increased n- or p-type doping. The G peak nearly symmetrically shifts to higher wave numbers regardless of the doping type, while the 2D peak shifts to lower (higher) wave numbers for n-type (p-type) doping. The wrinkles discussed here, however, display a shift of the 2D peak but not the G peak. Das et al. found that the shift of the 2D peak due to n-type doping by electrostatic gating became more prominent at high doping levels while the shift of the G peak saturated.[10] Additionally, they observed a decrease in the ratio I_{2D}/I_G at high n- or p-type doping, with the value dropping below unity for electron or hole concentrations above approximately 2×10^{13} cm^{-2}. These observations indicate a high level of doping in the graphene film in this study and may also help explain the relatively low I_{2D}/I_G observed in this work. Electronic measurements of other graphene films fabricated with the same procedure reliably exhibit Dirac points greater than 30 V using a back gate and 90 nm SiO_2, indicating strong p-type doping in as-fabricated CVD graphene films. Together, these observations suggest that the film is primarily p-doped while wrinkles are n-doped. Interestingly, the map of the 2D peak position of the graphene on copper is featureless. This suggests that if doping is in fact responsible for the 2D peak shift of the wrinkles in the transferred film, the wrinkles must become doped either during the copper etching or transfer process. Because the iron chloride solution used to etch the copper is highly oxidative, it is feasible that the etchant dopes the graphene film p-type but cannot reach certain areas of graphene which are folded up in the wrinkles. This does not, however, explain why the wrinkles would be heavily n-doped. In addition to doping, strain has also been shown to cause shifts in the G and 2D peaks.[12] This is not expected to be the dominant mechanism, however, due to the absence of a G peak shift, which is expected to occur in conjunction with a 2D shift. The mechanism behind the observed trend is not understood at this point, and further studies are needed.

Grain boundaries have been reported to appear solely in the Raman map of the D peak intensity due to the presence of structural disorder at the location of merged grains.[5,6,13] The map of D peak intensity in this work, however, has no variation except for some portions of the large creases. The reason that the grain boundaries are not visible is suspected to be because the grain size is smaller than the excitation laser beam spot. The average grain size can be estimated based on I_D/I_G according to the equation:

$$L_a(\text{nm}) = (2.4 \times 10^{-10})\lambda_{\text{laser}}{}^4 \left(\frac{I_D}{I_G}\right)^{-1} \quad (1)$$

where λ_{laser} is the laser wavelength in nanometers.[14] This yields an average grain size of 278 nm. Given that the laser beam spot is as small as 330 nm (provided by WITec) and the Raman spectra are taken at a rate of 8 points per micrometer, the absence of grain boundaries in the Raman maps is consistent with this estimate of grain size.

With the above understanding of the graphene film structure, the carrier diffusion was then studied. For this measurement, a 100-fs laser pump pulse with a central wavelength of 756 nm was tightly focused to the graphene film with a spot size (fwhm) of 2.3 μm. This excites electrons to the conduction band by interband absorption. A 100-fs probe pulse with a central wavelength of 1734 nm and a spot size of 3 μm is then used to detect these injected carriers at a given probe delay via differential transmission, defined as $\Delta T/T_0 = (T - T_0)/T_0$, where T and T_0 are the transmission with and without the presence of the pump pulse, respectively. When the pump pulse is present, the transmission of the probe pulse will be increased because of the population of some excited states by the pump pulse. The differential transmission of the probe pulse induced by the carriers is measured by using a mechanical chopper to modulate the pump beam intensity at a few kilohertz and detecting the transmitted probe with a photodiode and a lock-in amplifier referenced to the modulation frequency. The differential transmission signal is proportional to the carrier density at the probing energy and therefore can be used to monitor the carriers. Since the laser spot sizes are about 10 times larger than typical grain sizes but smaller than typical wrinkle and crease domains, the measurement results must be due to either wrinkles or creases, while the effect will be one of averaging over many grains. Using recently developed techniques to study carrier diffusion in various positions in this area,[15] the differential transmission signal is measured as we scan the probe spot across the pump spot with a fixed probe delay. This yields a spatial distribution of the carriers at that probe delay. Since the laser spots have Gaussian shapes, the initial distribution of carriers is Gaussian. Diffusion of carriers within the graphene film will cause the size of the distribution to increase. Quantitatively, the squared width increases linearly with time, with a slope determined by the diffusion coefficient[15] according to the equation

$$\omega^2(t) = \omega^2(0) + 16\ln(2)Dt \quad (2)$$

where ω is the width of the carrier distribution and D is the diffusion coefficient. The squared width can be deduced by a Gaussian fit of the measured carrier profiles and plotted as a function of time in order to extract D, the diffusion coefficient.

In order to study the influence of the crease on carrier dynamics, measurements of diffusion coefficient at four locations are shown in Figure 2, represented by the black circles in Figure 1a. Figure 2a is measured away from any creases, and Figures 2b–d sequentially approach the wishbone shaped intersection of creases with each subsequent point containing an increasing contribution from the creases. At every position the carrier behavior is best modeled by two separate diffusion coefficients: one for short probe delay times of up to 0.6–1 ps, denoted D_1, and one for longer probe delays, denoted D_2. As the excitation site approaches the crease intersection, both D_1 and D_2 decrease. At every position there is a clear, significant broadening of the carrier density profile owing to the diffusion of carriers. Although the diffusion equation predicts an overall linear increase of the squared width of the profile, there appears to be two time ranges with different slopes. The initial fast expansion is followed by a seemingly slower one. Recently, the nature of the transient absorption signal at late probe delays (i.e., >1 ps) in CVD graphene has been studied.[16] This recent study showed that such a slow component might be induced by extrinsic agencies in the samples which can be removed by prolonged laser exposure. The profiles measured at late probe delays could be a superposition of a fast-expanding profile induced by the charge carriers and a nonexpanding profile caused by these extrinsic agencies. This can give rise to an apparently slower expansion. However, at early probe delays the carrier contribution dominates and the expansion accurately reflects the carrier diffusion. Hence, in the following we will focus on the initial expansion and D_1 only.

To further separate the role of the wrinkles and creases, D_1 was measured in two linear scans over a second region of graphene, presented in Figure 3. Figure 3a shows an optical

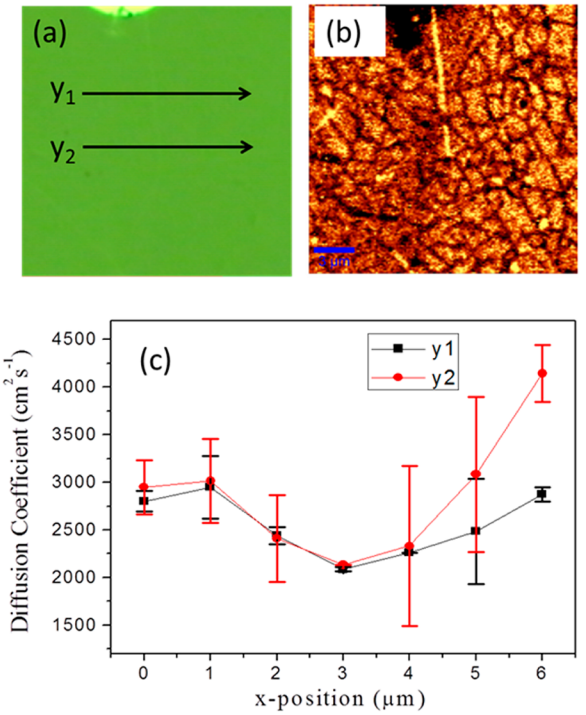

Figure 3. (a) Optical image of the region of interest. The two scanned lines are marked with black arrows. (b) Raman map of the ratio I_{2D}/I_G in the region shown in part a. The scale bar is 6 μm. (c) Map of diffusion coefficient D_1 versus position along scans y_1 and y_2.

microscope image of the area of interest. The curved bright feature at the top of the image is part of a titanium alignment marker. The two black horizontal lines denoted y_1 and y_2 are separated by 1 μm and represent scans of the diffusion coefficient D_1. Each line contains seven data points with a step size of 1 μm. The far left point is denoted as position 0 μm. A crease runs through the center of the scan, at the 3 μm position.

The crease is clearly visible as the vertical bright yellow line in the Raman map of I_{2D}/I_G in Figure 3b. Also visible are wrinkles separating regions of a few micrometers in size. Diffusion coefficient D_1 is plotted against position in Figure 3c for both scans y_1 and y_2. It is clear that the diffusion is worst when the pump pulse is directly on top of the crease. Interestingly, the differential transmission decay time constants (not shown) show no clear trend relative to position, suggesting that the crease does not affect carrier lifetime.

dx.doi.org/10.1021/am401518y | ACS Appl. Mater. Interfaces 2013, 5, 7176–7180

Scans y_1 and y_2 yield similar diffusion coefficients at all points except for position 6 μm. Since the probe beam spot is 3 μm in diameter, scans y_1 and y_2 will both contain information from a shared central horizontal strip. Scan y_1 (y_2) will also contain information from a strip above (below) the central strip of graphene film. The close overlap of the two data sets is not surprising since the crease runs equally through both scans.

The clear difference in D_1 between scans y_1 and y_2 at position 6 μm is interesting. One possible explanation for this difference could be the presence of wrinkles, as follows. The wrinkles may serve as obstacles that decrease the diffusion of charge carriers, particularly if they are charged relative to the surrounding graphene film. The typical wrinkle domain size in this region is approximately the size of the probe beam spot. For this reason, the points in scans y_1 and y_2 are likely to have very similar fractional areas consisting of wrinkles. At positions 5 and 6 μm, however, it is possible that y_2 may by chance probe an area entirely or nearly within a single wrinkle domain. This would imply that carriers can diffuse farther before encountering a wrinkle, leading to a 50% increase in diffusion coefficient for positions 6 μm. One interesting consequence of this hypothesis is that the effect of the crease is comparable or smaller than the effect of the wrinkles on the carrier diffusion judging by the size of the dip in the center of this curve at the position of the crease. This may be because the creases consist of folds and bends in the graphene film which may not alter the electronic structure much. The wrinkles on the other hand form at higher temperatures in a more dynamic process and may be doped relative to the surrounding graphene or consist of very sharp folds.

CONCLUSION

To summarize, the microstructure of transferred graphene grown by CVD on copper was studied with Raman spectroscopy and correlated with optical measurements of carrier diffusion. By avoiding patterning the film and depositing metal electrodes, several complicating factors are avoided. We found that, in addition to grain boundaries, wrinkles formed during cooling after graphene growth and creases from the transfer process both affect carrier diffusion by comparable amounts. Additionally, it was suggested that wrinkles may be heavily doped oppositely than the rest of the graphene film. This could be due to the oxidizing nature of the copper etchant which also contacts the graphene film. This work presents a powerful technique which can be used to understand the effect of defect structure on electronic properties of graphene films. With the great recent advances in characterizing the structure of different types of grain boundaries and the ability to grow macroscopic grains, much could be learned from extending this technique to ultrahigh quality graphene films with well-characterized grain boundaries.

AUTHOR INFORMATION

Corresponding Author

*E-mail: crochfo@sandia.gov (C.R.); jwu@ku.edu (J.W.).

Present Address

†C.R.: Sandia National Laboratories, Albuquerque, NM 87185, USA.

Notes

The authors declare no competing financial interest.

ACKNOWLEDGMENTS

The authors acknowledge support in part by ARO contract no. W911NF-12-1-0412 and NSF contract nos. NSF-DMR-1105986 and NSF EPSCoR-0903806 and matching support from the State of Kansas through Kansas Technology Enterprise Corporation. C.R. would like to acknowledge a National Science Foundation Graduate Research Fellowship. Sandia National Laboratories is a multiprogram laboratory managed and operated by Sandia Corporation, a wholly owned subsidiary of Lockheed Martin Corporation, for the United States Department of Energy's National Nuclear Security Administration under Contract DE-AC04-94AL85000.

REFERENCES

(1) Li, X.; Cai, W.; An, J.; Kim, S.; Nah, J.; Yang, D.; Piner, R.; Velamakanni, A.; Jung, I.; Tutuc, E.; Banerjee, S. K.; Colombo, L.; Ruoff, R. S. *Science* **2009**, *324*, 1312−1314.

(2) Liu, J.; Xu, G.; Rochford, C.; Lu, R.; Wu, J.; Edwards, C. M.; Berrie, C. L.; Chen, Z.; Maroni, V. A. *Appl. Phys. Lett.* **2011**, *99*, 023111.

(3) Bao, W.; Miao, F.; Chen, Z.; Zhang, H.; Jang, W.; Dames, C.; Lau, C. N. *Nat. Nanotechnol.* **2009**, *4*, 562−566.

(4) Ogawa, Y.; Hu, B.; Orofeo, C. M.; Tsuji, M.; Ikeda, K.; Mizuno, S.; Hibino, H.; Ago, H. *J. Phys. Chem. Lett.* **2011**, *3*, 219−226.

(5) Jauregui, L. A.; Cao, H.; Wu, W.; Yu, Q.; Chen, Y. P. *Solid State Commun.* **2011**, *151*, 1100−1104.

(6) Yu, Q.; Jauregui, L. A.; Wu, W.; Colby, R.; Tian, J.; Su, Z.; Cao, H.; Liu, Z.; Pandey, D.; Wei, D.; Chung, T. F.; Peng, P.; Guisinger, N. P.; Stach, E. A.; Bao, J.; Pei, S.-S.; Chen, Y. P. *Nat. Mater.* **2011**, *10*, 443−449.

(7) Wei, D.; Liu, Y.; Wang, Y.; Zhang, H.; Huang, L.; Yu, G. *Nano Lett.* **2009**, *9*, 1752−1758.

(8) Ni, Z. H.; Yu, T.; Luo, Z. Q.; Wang, Y. Y.; Liu, L.; Wong, C. P.; Miao, J.; Huang, W.; Shen, Z. X. *ACS Nano* **2009**, *3*, 569−574.

(9) Wang, Y. Y.; Ni, Z. H.; Shen, Z. X.; Wang, H. M.; Wu, Y. H. *Appl. Phys. Lett.* **2008**, *92*, 043121.

(10) Das, A.; Pisana, S.; Chakraborty, B.; Piscanec, S.; Saha, S. K.; Waghmare, U. V.; Novoselov, K. S.; Krishnamurthy, H. R.; Geim, A. K.; Ferrari, A. C.; Sood, A. K. *Nat. Nanotechnol.* **2008**, *3*, 210−215.

(11) Yan, J.; Zhang, Y.; Kim, P.; Pinczuk, A. *Phys. Rev. Lett.* **2007**, *98*, 166802.

(12) Mohiuddin, T. M. G.; Lombardo, A.; Nair, R. R.; Bonetti, A.; Savini, G.; Jalil, R.; Bonini, N.; Basko, D. M.; Galiotis, C.; Marzari, N.; Novoselov, K. S.; Geim, A. K.; Ferrari, A. C. *Phys. Rev. B* **2009**, *79*, 20543.

(13) Song, H. S.; Li, S. L.; Miyazaki, H.; Sato, S.; Hayashi, K.; Yamada, A.; Yokoyama, N.; Tsukagoshi, K. *Sci. Rep.* **2012**, *2*, 337.

(14) Pimenta, M. A.; Dresselhaus, G.; Dresselhaus, M. S.; Cançado, L. G.; Jorio, A.; Saito, R. *Phys. Chem. Chem. Phys.* **2007**, *9*, 1276−1290.

(15) Ruzicka, B. A.; Wang, S.; Werake, L. K.; Weintrub, B.; Loh, K. P.; Zhao, H. *Phys. Rev. B* **2010**, *82*, 195414.

(16) Ruzicka, B. A.; Wang, S.; Liu, J.; Loh, K.-P.; Wu, J. Z.; Zhao, H. *Opt. Mater. Express* **2012**, *2*, 708−716.